# Systematic study of foreign-atom-doped fullerenes by using a nuclear recoil method and their MD simulation



doi: 10.1063/1.480858

# Systematic study of foreign-atom-doped fullerenes by using a nuclear recoil method and their MD simulation

T. Ohtsuki
*Laboratory of Nuclear Science, Tohoku University, Mikamine, Taihaku-ku, Sendai 982-0826, Japan*

K. Ohno, K. Shiga, and Y. Kawazoe
*Institute for Materials Research, Tohoku University, Katahira, Aoba-ku, Sendai 980-8577, Japan*

Y. Maruyama
*National Industrial Research Institute of Nagoya (NIRIN), 1-1 Hirate-cho, Kita-ku, Nagoya, 462-8510, Japan*

K. Masumoto
*Radiation Science Center, High Energy Accelerator Research Organization, Tanashi, Tokyo, 188-8501, Japan*

(Received 17 August 1999; accepted 10 November 1999)

The formation of atom-doped fullerenes has been investigated by using several types of radionuclides produced by nuclear reactions. It was found that the endohedral fullerenes ($Kr@C_{60}$, $Xe@C_{60}$) and their dimers, furthermore, heterofullerenes, such as $AsC_{59}$, $GeC_{59}$ and their dimers, are produced by a recoil process following nuclear reactions. Other nuclear reaction products (Na, Ca, Sc, etc.) may destroy most of the fullerene cage in the same process. Carrying out *ab initio* molecular-dynamics simulations based on an all-electron mixed-basis approach, we confirmed that the formation of Kr- (or Xe-) atom-doped endohedral fullerenes and of substitutional heterofullerenes doped with an As atom is really possible. The experimental and theoretical results indicate that the chemical nature of doping atoms is important in the formation of foreign-atom-doped fullerenes. © *2000 American Institute of Physics.* [S0021-9606(00)00506-7]

## I. INTRODUCTION

Since the discovery of fullerenes[1] and the synthesis of a large amount of fullerenes,[2] numerous experimental and theoretical studies for endohedrally doped,[3–10] exohedrally doped[11–13] as well as heterofullerenes[14–20] involving foreign atoms have been presented. Such species have typically been produced by using arc-desorption or laser-vaporization techniques, but the doping of atoms *a posteriori* into already created fullerenes has been attempted using several methods. Saunders *et al.*[21] demonstrated the possibility of the incorporation of noble-gas atoms into fullerenes under high-pressure and high-temperature conditions, Braun *et al.*[22,23] and Gadd *et al.*[24] tried to produce atom-doped $C_{60}$ by using the prompt-gamma recoil induced by neutron irradiation followed by removal of damaged or incomplete fusion products using HPLC (high-pressure liquid chromatography). However, only partial evidence of atom-doped fullerenes has been presented so far. In our previous studies,[25–29] we found that not only the fullerenes substitutionally doped with $^{11}C$, such as $^{11}CC_{59}$ and $^{11}CC_{69}$, but also their dimers were produced by irradiation of already created fullerene cages with high-energy Bremsstrahlung or charged particles. Recently, we confirmed that endohedrally doped atoms[30,31] were produced by the recoil process following nuclear reactions. This earlier work suggested that the successful production of endohedral fullerenes is limited to small ion-radius atoms and chemically inert noble-gas atoms[30–32] which can pass through the tight six- or five-membered rings.

In the present study, we examine the production of fullerene derivatives created when alkali and alkali-earth (Na, Ca), transition metals (Sc, V, Cr, Mn, Co, Ni, Zn), 3B~5B elements (Ga, Ge, and As) and noble-gas elements (Kr or Xe), were produced by nuclear reactions induced by irradiation of samples with high-energy Bremsstrahlung or charged particles. We found that 4B and 5B elements and noble-gas elements can be incorporated with fullerene cages, while alkali, alkali-earth and transitional metals cannot remain in the fullerene portion. In order to check the possibility of direct incorporation, we carried out *ab initio* molecular-dynamics (MD) simulations using our all-electron mixed-basis code.

## II. EXPERIMENTAL PROCEDURES

### A. Sample preparation

To produce the source of radioactive nuclides, several materials (for example, $Na_2CO_3$ powder, $^{48}CaCO_3$,... as listed in Table I), were used in powder form. The grain size of the materials was smaller than 300 meshes. Purified fullerenes, $C_{60}$ and/or $C_{70}$, were elaborately mixed with each material (weight ratio=1:1) in an agate mortar, adding a few ml of carbon disulfide ($CS_2$). After drying up, about 10 mg of the mixture sample was wrapped in a pure aluminum foil of 10 $\mu$m in thickness for irradiation.

 

TABLE I. Nuclear data and experimental condition for the foreign-atom-doped fullerenes.

| Nuclide produced | $\gamma$-ray[a] | Half-life | Reaction | Material[b] |
|---|---|---|---|---|
| $^{22}$Na | 1275 keV | 2.6 y | $^{23}$Na($\gamma$,$n$)$^{22}$Na | $C_{60}+Na_2CO_3$ |
| $^{47}$Ca | 1297 keV | 4.5 d | $^{48}$Ca($\gamma$,$n$)$^{47}$Ca | $C_{60}+^{48}CaCO_3$[c] |
| $^{48}$Sc | 984 keV | 43.7 h | $^{48}$Ca($d$,2$n$)$^{48}$Sc | $C_{60}+^{48}CaCO_3$[c] |
| $^{48}$V | 984 keV | 16.0 d | $^{48}$Ti($d$,2$n$)$^{48}$V | $C_{60}$+Ti |
| $^{51}$Cr | 320 keV | 27.7 d | $^{51}$V($d$,2$n$)$^{51}$Cr | $C_{60}$+VC |
| $^{52}$Mn | 936 keV | 5.6 d | $^{52}$Cr($d$,2$n$)$^{52}$Mn | $C_{60}$+Cr |
| $^{56}$Co | 847 keV | 78.8 d | $^{56}$Fe($d$,2$n$)$^{56}$Co | $C_{60}+Fe_2O_3$ |
| $^{57}$Ni | 1378 keV | 36.0 h | $^{58}$Ni($\gamma$,$n$)$^{57}$Ni | $C_{60}$+NiO |
| $^{65}$Zn | 1115 keV | 244 d | $^{65}$Cu($d$,2$n$)$^{65}$Zn | $C_{60}$+CuO |
| $^{66}$Ga | 1039 keV | 9.4 h | $^{66}$Zn($d$,2$n$)$^{66}$Ga | $C_{60}$+Zn |
| $^{69}$Ge | 511 keV | 39.6 h | $^{69}$Ga($d$,2$n$)$^{69}$Ge | $C_{60}+Ga_2O_3$ |
| $^{72}$As[d] | 511 keV | 26 h | $^{72}$Ge($d$,2$n$)$^{72}$As | $C_{60}$+GeO |
| $^{79}$Kr | 261 keV | 34.9 h | $^{79}$Br($d$,2$n$)$^{79}$Kr | $C_{60}$+KBr |
| $^{127}$Xe | 203 keV | 36.4 h | $^{127}$I($d$,2$n$)$^{127}$Xe | $C_{60}$+KBr |

[a]Most abundant $\gamma$-ray is listed here (Ref. 33).
[b]Irradiated material as a target.
[c]Enriched $^{48}$Ca was used here.
[d]Other radioisotopes, such as $^{71}$As and $^{74}$As can also be produced by ($d$,$n$) or ($d$,2$n$) reactions. Only the abundant radioisotope $^{72}$As is listed.

### B. Charged-particle and high-energy Bremsstrahlung irradiation

According to the source nuclide used, either charged-particle or high-energy Bremsstrahlung irradiation was used. In Table I, the radionuclide produced, its characteristic $\gamma$-ray, its half-life, and the nuclear reaction are listed for each target material.

Deuteron irradiation with a beam energy of 16 MeV was performed at the Cyclotron Radio-Isotope Center, Tohoku University. The beam current was typically 5 $\mu$A and the irradiation time was about 1 hour. The sample was cooled with He-gas during irradiation.

Several radioisotopes of As can be produced by ($d$,$n$) or ($d$,2$n$) reactions with a bombardment on natural Ge. Here, we paid attention to the radioactivity of $^{72}$As ($^{71}$As, $^{74}$As), as shown in Table I, for reason of the appropriate half-lives and of the abundance of the $\beta^+$ decay rate for counting the 511 keV annihilation $\gamma$-ray.

For production of a doping nuclide such as $^{22}$Na, $^{47}$Ca or $^{57}$Ni, a sample was set in a quartz tube and irradiated with Bremsstrahlung of $E_{max}$=50 MeV which originated from the bombardment of a Pt plate of 2 mm in thickness with an electron beam provided by a 300 MeV electron linac at the Laboratory of Nuclear Science, Tohoku University. The beam current was typically 120 $\mu$A and the irradiation time was about 8 hours. The samples were also cooled in a water bath during the irradiation.

After irradiation, the samples were left for one day to allow several kinds of short-lived radioactive by-products to decay.

### C. Chemical separation and $\gamma$-ray measurement

The sample was dissolved in *o*-dichlorobenzene and filtered through a millipore filter (pore size=0.2 and/or 0.45 $\mu$m) to remove insoluble materials. The soluble portion was injected into a HPLC device equipped with a 5PBB (Cosmosil) (silica-bonded with a pentabromobenzyl group) column of 10 mm (in inner diameter)×250 mm (in length) at a flow rate of 3 or 4 ml/min in each run. For the confirmation of fullerenes and their derivatives, a UV detector was installed with a wavelength of 290 nm. Downstream of the UV detector, two $\gamma$-ray detectors consisting of a bismuth-germinate scintillator and of a photomultiplier (BGO-PM) were used to count the 511 keV annihilation $\gamma$-rays emanating from $^{69}$Ge and $^{72}$As ($^{71}$As, $^{74}$As) in coincidence. Data from the radiochromatogram were accumulated by means of a multichannel scaler system (MCS), using a personal computer. In order to measure the $\gamma$-rays emanating from other radionuclides, eluent fractions were collected for 30 s intervals (0–30, 30–60, 60–90,... s), and the $\gamma$-ray activities of each fraction were measured with a Ge detector coupled to a 4096-channel pulse-height analyzer, the conversion gain of which was set at 0.5 keV per channel. The energy resolution of the Ge detector was 1.8 keV in FWHM at the photopeak of 1332 keV of the $^{60}$Co source. Therefore, each nuclide listed in Table I could be uniquely detected by means of its characteristic $\gamma$-ray, and any other sources were ruled out. A schematic view of the radiochromatograph system is shown in Fig. 1.

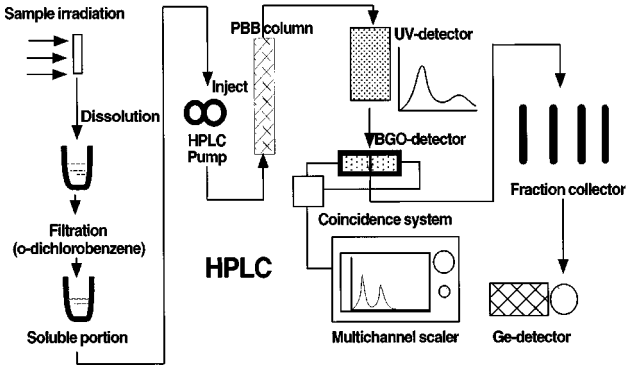


FIG. 1. Schematic view of the radiochromatograph system. Column; 5PBB, UV detector; 290 nm wavelength, solvent; *o*-dichlorobenzene, flow rate 3 or 4 ml/min. To measure the 511 keV annihilation $\gamma$-rays from $^{72}$As and $^{69}$Ge with the two BGO detectors, a capillary loop was used to obtain sufficient statistical data for the $\gamma$-rays. Geometrical efficiency for coincident counting of the $\gamma$-rays was estimated to be about 30%. Furthermore, to measure the $\gamma$-rays emanating from objective radionuclides by using a Ge-detector, eluent fractions were collected automatically.

## III. RESULTS

### A. Radiochromatogram of alkali, alkali-earth and transition metals: Na, Ca, Sc, V, Cr, Mn, Co, Ni, and Zn

The elution curves shown by solid lines in Figs. 2(a) and 2(b) indicate the absorbances, which were monitored continuously by the UV detector for the irradiated samples of $C_{60}$ that were mixed with several materials (see Table I). The horizontal and vertical axes, respectively, indicate the retention time after their injection into the HPLC and the absorption intensity of the UV as well as the $\gamma$ counting rate of the radionuclide being produced.

Strong UV absorption occurs at 7.0–8.5 min in Figs. 2(a) and 2(b). This peak position in both figures corresponds to the retention time of $C_{60}$, which was determined by the

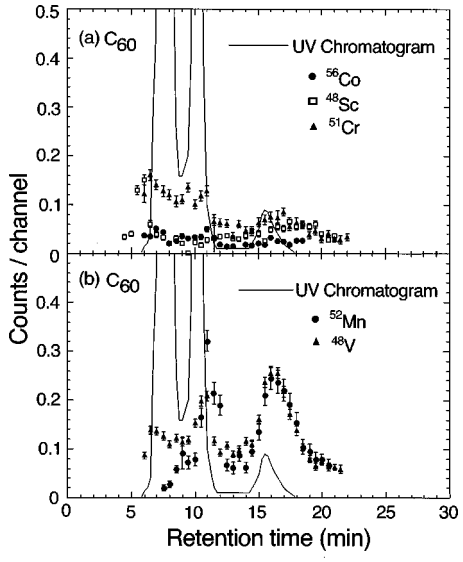


FIG. 2. (a) HPLC elution curves of the soluble portion of the crude extracted in the deuteron-irradiated sample of $C_{60}$ which was mixed with $Fe_2O_3$, $CaCO_3$ or VC. The horizontal axis indicates retention time, while the vertical axis represents the counting rate of the radioactivity of $^{56}Co$ (closed circle), $^{48}Sc$ (open square), and $^{51}Cr$ (closed triangle) in each fraction as well as the absorbance in a UV chromatogram of $C_{60}$ (solid line, arbitrary unit). Error bars indicate the statistical error of the $\gamma$ counting rate. (b) Same as (a), but for the deuteron-irradiated sample of $C_{60}$ mixed with Ti or Cr. The symbols indicate the $\gamma$-counting rate of the radioactivity of $^{52}Mn$ (closed circle) and of $^{48}V$ (closed triangle). Error bars also indicate the statistical error of the $\gamma$-counting rate. Two peaks (11 min and 15–18 min), respectively, indicate the formation of $^{52}Mn@C_{60}-C_{60}$ ($^{48}V@C_{60}-C_{60}$) and $^{52}Mn@C_{60}-(C_{60})_2$ ($^{48}V@C_{60}-(C_{60})_2$).

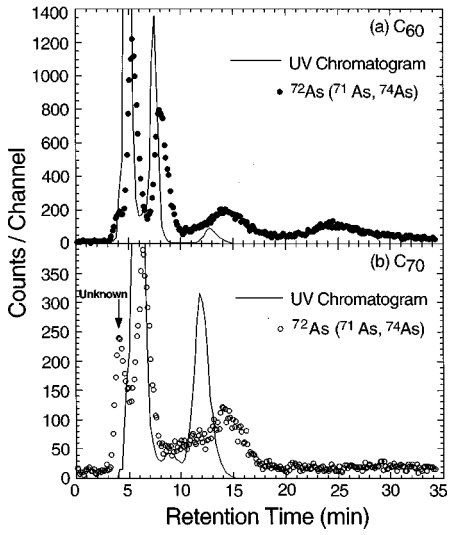


FIG. 3. (a) Same as Fig. 2 but for the deuteron-irradiated sample of $C_{60}$ mixed with GeO. The horizontal axis indicates retention time, while the vertical axis represents the $\gamma$-counting rate (closed circles) of the radioactivities of $^{72}As$ ($^{71}As$, $^{74}As$), as measured with a BGO detector in coincidence, and the absorbance of a UV chromatogram of $C_{60}$ (solid line, arbitrary unit). Four peaks (4.5–6 min, 7–10 min, 12–18 min, and 21–30 min), respectively, indicate the formation of $^{72}AsC_{59}$, $^{72}AsC_{59}-C_{60}$, and $^{72}AsC_{59}-(C_{60})_2$ as well as $^{72}AsC_{59}-(C_{60})_3$. (b) Same as (a) but for the radiochromatography for the deuteron-irradiated sample of $C_{70}$+GeO. Open circles also indicate the populations of $^{72}As$ ($^{71}As$, $^{74}As$). The second and third peaks (5–8 min, 12–17 min), respectively, indicate the formation of $^{72}AsC_{69}$, $^{72}AsC_{69}-C_{70}$.

calibration run using the $C_{60}$ sample before the irradiation. Furthermore, a second (9.5–10.5 min) peak and a small third (14–18 min) one were observed in the UV chromatogram of the $C_{60}$ sample. These peaks seem to be larger molecules than $C_{60}$. For the characterization of the components, the fraction corresponding to the second peak in the irradiated sample of $C_{60}$ was collected and examined with MALDI TOF (matrix-assisted laser-desorption ionization time-of-flight) mass spectrometry in a separate run. The mass spectrum of the fraction exhibited a series of peaks at $m/z1440-24n$ ($n=1-4$) corresponding to the molecular ion peak of $C_{120}-nC_2$, in addition to the peak for $C_{60}$ as a base peak.[29] Therefore, the second (9.5–10.5 min) peak and the small third (14–18 min) one of Fig. 2(a) could be, respectively, assigned to $C_{60}$ dimers and $C_{60}$ trimers. These materials (mostly nonradioactive polymers) can be produced by the interaction between $C_{60}$'s in coalescence reactions after ionization by incident deuterons or by the charged particles being produced.[29] A similar trend has been observed in our previous study of radioactive fullerenes labeled with $^{11}C$.[25,26]

Closed circles, open squares, and open triangles in Fig. 2(a), respectively, indicate the $\gamma$-counting rate of $^{56}Co$, $^{48}Sc$, and $^{51}Cr$ in each eluent fraction, as measured with the Ge detector. It was found that no clear correlation exists in the elution behavior between the UV chromatogram and the radioactivity (population of each radionuclide; $^{56}Co$, $^{48}Sc$, $^{51}Cr$). Furthermore, no activities of $^{22}Na$, $^{47}Ca$, $^{57}Ni$, and $^{65}Zn$ were observed in the soluble portion of the crude material which was extracted after the solvation process.

Closed triangles and closed circles in Fig. 2(b), respectively, indicate the $\gamma$-counting rate of $^{48}V$ and $^{52}Mn$ of each eluent fraction, as measured with the Ge detector. There were two peaks of the $^{48}V$ ($^{52}Mn$) radioactivity at the retention times of around 11 min and of 15–18 min in Fig. 2(b) for the sample of $C_{60}$ which was mixed with Ti (Cr). Two peaks of the $^{48}V$ ($^{52}Mn$) radioactivity almost correspond to the dimer and trimer portions, as measured by the UV detector though there is a slight delay. But no clear peak of the $^{48}V$ ($^{52}Mn$) radioactivity was evident around the first peak (7–8.5 min) of the UV chromatogram which is fullerene monomer population.

### B. Radiochromatogram of 3B–5B elements: Ga, Ge, and As

#### *1. 5B element (As)*

Figures 3(a) and 3(b), respectively, show the two elution curves of the $C_{60}$+GeO and $C_{70}$+GeO samples irradiated by deuterons of $E_d=16$ MeV. In the figure, the time delay of the BGO chromatogram in relation to the UV was corrected by the flow rate and the capillary length between the UV and the BGO detectors.

In Fig. 3(a), a strong absorption peak was observed at the retention time of 4.5–5.5 min along the elution curve (the solid line) which was measured by a UV detector. This peak indicates the existence of $C_{60}$. Following the first peak, two peaks at around 7–8 min and 11–15 min were consecutively observed in the UV chromatogram. This fact indicates that the second peak and the smaller third one can also be as-

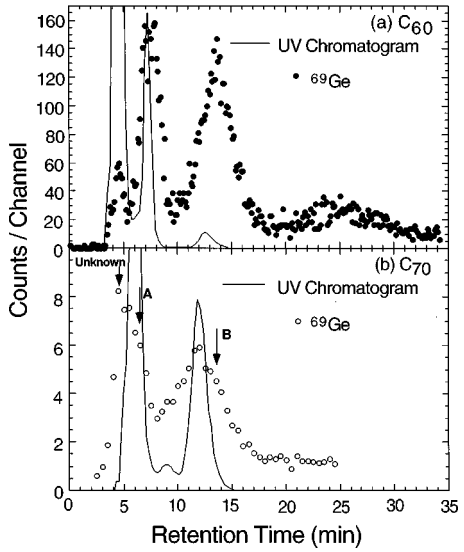


FIG. 4. (a) Same as Fig. 2 but for the deuteron-irradiated sample of $C_{60}$ mixed with $Ga_2O_3$. The horizontal axis indicates retention time, while the vertical axis represents the $\gamma$-counting rate of the radioactivity of $^{69}$Ge (closed circle), as measured with a BGO detector, and the absorbance of a UV chromatogram of $C_{60}$ (solid line, arbitrary unit). Four peaks (4–5 min, 6–9 min, 11–17 min, and 21–30 min) indicate the formation of $^{69}GeC_{59}$, $^{69}GeC_{59}$–$C_{60}$, and $^{69}GeC_{59}$–$(C_{60})_2$ as well as $^{69}GeC_{59}$–$(C_{60})_3$. (b) Same as (a) but for the radiochromatography for the deuteron-irradiated sample of $C_{70}$+$Ga_2O_3$. The open circle indicates the populations of $^{69}$Ge. In the figure, two peaks around A (6–7 min) and B (12–17 min) may, respectively, indicate the formation of $^{69}GeC_{69}$ , $^{69}GeC_{69}$–$C_{70}$.

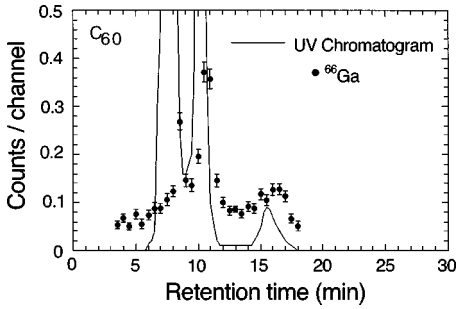


FIG. 5. Same as Fig. 2 but for the deuteron-irradiated sample of $C_{60}$ mixed with Zn. The horizontal axis indicates retention time, while the vertical axis represents the counting rate of the radioactivity of $^{66}$Ga, as measured with a Ge detector and the absorbance of a UV chromatogram of $C_{60}$ (solid line, arbitrary unit). Error bars also indicate the statistical error of the $\gamma$-counting rate. Three peaks (8.5 min, 9.5–11.5 min, and 14–18 min) may, respectively, indicate the formation of $^{66}Ga@C_{60}$ and $^{66}Ga@C_{60}$–$C_{60}$ as well as $^{66}Ga@C_{60}$–$(C_{60})_2$.

signed, respectively, to the $C_{60}$ dimers and $C_{60}$ trimers. Four peaks appeared along the curve of the radioactivity of $^{72}$As ($^{71}$As, $^{74}$As) in the radiochromatogram when the $C_{60}$ sample (a mixture of $C_{60}$ and GeO) was irradiated. Aside from a slight delay, the first peak (4.5–6 min) corresponds to the UV absorption peak of $C_{60}$. A second peak as well as relatively broad third and fourth peaks were observed, respectively, at the retention times of 7–10 min, 12–18 min, and 21–30 min. Though there is also a delay in the elution peaks of the radioactivity in comparison with those of the UV absorption peaks, it seems that the elution behavior is similar. This result indicates that the radioactive fullerene monomers of $C_{60}$ and their polymers labeled with $^{72}$As ($^{71}$As, $^{74}$As) possibly exist in the fullerene portion.

For a sample produced by irradiating a mixture of $C_{70}$ and GeO, two strong absorption peaks of the UV were also observed at 4.5–7 min and 10–14 min. We attribute these peaks to the presence of $C_{70}$ monomers and dimers, respectively [see the solid line of Fig. 3(b)]. Three peaks of the radioactivity of $^{72}$As ($^{71}$As, $^{74}$As) were revealed in the chromatogram (see the open circles). The first peak (3–5 min) is an unknown byproduct that lacks a UV absorption peak around the same retention time. The second (5–8 min) peak and a broad third (12–17 min) one may indicate the existence of the radioactive fullerene monomers of $C_{70}$ and of their dimers labeled with $^{72}$As ($^{71}$As, $^{74}$As).

### 2. 4B element (Ge)

Figures 4(a) and 4(b) show the elution behavior of $^{69}$Ge was investigated for irradiated samples of $C_{60}$+$Ga_2O_3$ and $C_{70}$+$Ga_2O_3$. A similar trend was observed in the elution behavior between the radioactivities of $C_{60}$ and $^{69}$Ge, as seen in Fig. 3(a), though the first peak (4–5 min) of the $^{69}$Ge radioactivity was relatively smaller than that for $^{72}$As ($^{71}$As, $^{74}$As). Therefore, the radioactive fullerene monomers of $C_{60}$ and their polymers labeled with $^{69}$Ge possibly exist in the fullerene portion.

A relationship of the elution behavior between the radioactivities of $C_{70}$ and $^{69}$Ge was also shown in Fig. 4(b). Two broad peaks were observed in the chromatogram. These two populations may contain some unknown by-products since the peaks of the populations ($^{69}$Ge) appear rather earlier than the peaks of the UV. Therefore, the portions of the shoulders ''A'' and ''B'' denoted in the figure may indicate the existence of the radioactive fullerene monomers of $C_{70}$ and of their dimers labeled with $^{69}$Ge, because a slight delay of the populations is certainly observed, as seen in Figs. 3(a) and 3(b).

### 3. 3B element (Ga)

The elution curves shown by a solid line and closed circles in Fig. 5 indicate the UV absorbance, and the $\gamma$-counting rate of $^{66}$Ga (as measured by the Ge detector), respectively. Here the radionuclides ($^{66}$Ga) were produced by the irradiation of a sample of $C_{60}$+Zn. Three components (7–8.5 min, 9.5–10.5 min, and 14–18 min) in the UV chromatogram can also be attributed, respectively, to $C_{60}$ monomers, their dimers and their trimers. Three populations of $^{66}$Ga appear at the retention times of 8.5 min, 9.5–11.5 min and 14–18 min in Fig. 5, respectively, though the amount of the radioactivity seems to be much less than that of $^{72}$As ($^{71}$As, $^{74}$As) and $^{69}$Ge.

## C. Radiochromatogram of noble-gas elements: Kr

Three peaks appear in the UV chromatogram of material from an irradiated sample of $C_{60}$+KBr, as seen in Fig. 6(a). TOF-mass measurement indicated that the second (7.5–9.5 min) peak and a small third (12–16 min) one of Fig. 6(a) could be assigned, respectively, to $C_{60}$ dimers and trimers. Two peaks appear in the UV chromatogram in the irradiated

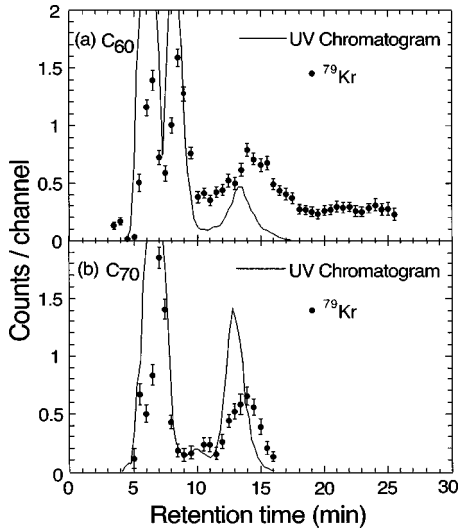


FIG. 6. Same as Fig. 2 but for the deuteron-irradiated sample of $C_{60}$ mixed with KBr. The horizontal axis indicates retention time, while the vertical axis represents the counting rate of the radioactivities of $^{79}$Kr in each fraction (closed circle) and the absorbance of a UV chromatogram of $C_{60}$ (solid line, arbitrary unit). Error bars indicate the statistical error of the $\gamma$-counting rate. Three peaks (5–7 min, 7.5–10 min, and 12–18 min), respectively, indicate the formation of $^{79}Kr@C_{60}$ and $^{79}Kr@C_{60}-C_{60}$ as well as $^{79}Kr@C_{60}-(C_{60})_2$. (b) Same as (a) but for the sample of $C_{70}$ mixed with KBr. Two peaks (6–8 min and 11.5–16 min), respectively, indicate the formation of $^{79}Kr@C_{60}$ and $^{79}Kr@C_{60}-C_{60}$.

sample of $C_{70}$+KBr, as seen in Fig. 6(b). The second peak (11.5–16 min) was attributed to $C_{70}$ dimers. Closed circles in Figs. 6(a) and 6(b) indicate the radioactive counting rate of $^{79}$Kr for each eluent fraction, as measured with the Ge detector. There are three peaks of the $^{79}$Kr radioactivity at the retention times of about 5–7 min and 7.5–10 min, 12–18 min in Fig. 6(a), while two peaks of the $^{79}$Kr radioactivity occur at the retention times of about 6–8 min and 11.5–16 min in Fig. 6(b). Figures 6(a) and 6(b) both show clear correlations between the UV chromatograms (which measure fullerene populations) and the $^{79}$Kr radioactivities (which measure $^{79}$Kr populations). Therefore, the radioactive monomers of $C_{60}$ or $C_{70}$ and their polymers labeled with $^{79}$Kr possibly exist in the fullerene portions of these samples.

## IV. DISCUSSION

### A. Materials being produced

#### *1. Alkali, alkali-earth, transitional metals*

As seen in Fig. 2(a), no clear correlation was seen in the elution behavior between the UV and the population of radionuclides ($^{48}$Sc, $^{51}$Cr, $^{56}$Co). Furthermore, no activities of $^{22}$Na, $^{47}$Ca, $^{57}$Ni, and $^{65}$Zn were observed in the soluble portion of $C_{60}$. Therefore, the present results for the elements (Na, Ca, Sc, Cr, Co, Ni, and Zn) suggest that the attack converts the cage into incomplete fusion or non-fullerene materials and the most of these materials can be removed during the solvation process. However, a correlation of the elution behaviors between the UV chromatogram and the radioactivities of $^{48}$V ($^{52}$Mn) seems to be similar to the results for the formation of $Kr@C_{60}$ ($Xe@C_{60}$) and of their polymers [see Fig. 6(a) and Ref. 31], though no identical peak of the $^{48}$V ($^{52}$Mn) radioactivity was seen around the first peak of the UV chromatogram. Since alkali, alkali-earth, and transitional metals cannot combine covalently with the carbon atoms of a fullerene cage or are removed in the solvent if they are exohedral, this observation may corroborate the formation of endohedral dimer (and trimer) fullerenes with encapsulated $^{48}$V and $^{52}$Mn, namely $^{48}V@C_{60}-C_{60}$ and $^{48}V@C_{60}-(C_{60})_2$ and $^{52}Mn@C_{60}-C_{60}$ and $^{52}Mn@C_{60}-(C_{60})_2$ (for samples of $C_{60}$ mixed with Cr and Ti, respectively). The monomers, such as $M@C_{60}$ ($M=^{48}$V, $^{52}$Mn), could not be observed in the chromatogram. This fact may indicate that the shock of the collision is rather greater than that in the case of $^{79}$Kr ($^{127}$Xe) case and it induces the cages to coalesce with neighboring cages with a high degree of probability (formation of the dimer and trimer). Therefore, the magnitude of the chemical reactivity between atoms (alkali, alkali-earth, and transitional metals) and fullerenes seems to be much greater, even if the endohedral polymers are detected in some cases.

#### *2. 3B–5B elements*

From the correlation of the elution behaviors between the UV chromatogram and the radioactivity of an objective atom, we earlier found that several endohedral fullerenes, namely $^{7}Be@C_{60}$,[30] $^{127}Xe@C_{60}$,[31] and their dimers, can be produced by nuclear recoil implantation.

Though similar results were observed here in the elution behavior between the UV and the $^{72}$As ($^{71}$As, $^{74}$As) and $^{69}$Ge populations, the materials being produced seem to be somewhat different. Here, As- or Ge-doped heterofullerenes, as a part of the cage, can be observed by means of the radiochromatography. We present several reasons here for the formation of such atom-doped heterofullerenes: (1) 4B or 5B group elements, such as Ge or As, prefer a covalent bond (an $sp^3$-like bonding), and furthermore, evidence for Si-doped heterofullerenes has been presented, even if the bond structure is $sp^3$.[18,19] (2) Previously, we reported results concerning the formation of other radioactive fullerenes, $^{11}CC_{59}$ and $^{13}NC_{59}$, using the recoil-implantation process following nuclear reactions.[25,28] These results indicate that energetic $^{11}$C or $^{13}$N nuclides can be successfully incorporated in fullerene cages.[25,28] (3) We have confirmed the formation of endohedral fullerenes, namely $^{7}Be@C_{60}$,[30] $^{127}Xe@C_{60}$.[31] Furthermore, the formation of the atom-doped fullerenes has also been investigated in several radioisotopes (Na, Ca, Sc, V, Cr, Mn, Co, Ni, Zn), using the same method. It was also found that most of the elements could not be detected in the $C_{60}$ portion against the produced amount of the endohedral fullerenes (here, $^{127}Xe@C_{60}$ was produced at most $10^{10}$ molecules[31]). However, it is noted that the amount of $^{72}$As ($^{71}$As, $^{74}$As) and $^{69}$Ge, which remains in the final fullerene portion, is estimated to be several tens of times greater than that of endohedral fullerenes (i.e., $^{127}Xe@C_{60}$). This amount is rather closer to the production rate of $^{11}CC_{59}$.[29] Therefore, our observation may corroborate the formation of heterofullerenes with networked As* (the asterisk denotes $^{72}$As, $^{71}$As, $^{74}$As); namely $As^*C_{59}$ (monomers), $As^*C_{59}-C_{60}$ (dimers), $As^*C_{59}-(C_{60})_2$ (trimers), $As^*C_{59}-(C_{60})_3$ (tetramers), or further $As^*C_{69}$ (monomers), $As^*C_{69}-C_{70}$ (dimers)

when the sample of $C_{60}$+GeO or $C_{70}$+GeO was irradiated, respectively. These materials correspond to the $\gamma$-counting peaks which were measured with the BGO in Figs. 3(a) and 3(b). For the same reasons, materials being produced in the irradiation for the sample of $C_{60}+Ga_2O_3$ or of $C_{70}+Ga_2O_3$ can be assigned, respectively, to $^{69}GeC_{59}$ and to their polymers, or to $^{69}GeC_{69}$ and to their dimers. These materials also correspond to the $\gamma$-counting peaks which are measured with the BGO in Figs. 4(a) and 4(b), though some amount of the by-products may remain in the populations [see Fig. 4(b)].

Three populations of $^{66}$Ga were observed in the radiochromatogram in Fig. 5 when the sample of $C_{60}$+Zn was irradiated. Nevertheless, it should be noted that the radioactivity of $^{66}$Ga remaining in the soluble portion of $C_{60}$ is much less than the radioactivity of $^{72}$As ($^{71}$As, $^{74}$As), or of $^{69}$Ge. The amount of the $^{66}$Ga being produced with the incorporation of fullerenes is rather closer to that of $^{48}V@C_{60}$ ($^{52}Mn@C_{60}$). Furthermore, the elution behavior is similar to that of $^{48}V@C_{60}$ ($^{52}Mn@C_{60}$). Therefore, this result may corroborate the formation of $^{66}$Ga-doped endohedral fullerenes, such as $^{66}Ga@C_{60}$ and their dimers and trimers. This fact may indicate that the chemical nature of Ga is rather closer to transitional metals. However, further study is needed for verifying the materials, since B (boron), which belongs to the same group (3B element), can combine with the cage.[14,15]

#### 3. Noble-gas atom

A clear correlation between the elution behaviors of the $C_{60}$ and $C_{70}$ populations and the $^{79}$Kr populations, as seen in Figs. 6(a) and 6(b), indicates that the Kr atoms stop inside the $C_{60}$ and $C_{70}$ cages. The first peaks in Fig. 6(a) and 6(b) can be, respectively, assigned to $^{79}Kr@C_{60}$ and $^{79}Kr@C_{70}$, because such a noble gas cannot combine exohedrally or covalently with carbon atoms, even if the ion radius is greater than that of five- or six-membered rings. Furthermore, it seems that the shock of the collisions produces fullerene polymers by interacting with a neighboring fullerene cage. The observation of the second and third peaks in Fig. 6(a), respectively, corroborates the formation of endohedral fullerene dimers and trimers with encapsulated $^{79}$Kr; namely $^{79}Kr@C_{60}-C_{60}$ and $^{79}Kr@C_{60}-(C_{60})_2$. Likewise, the second peak in Fig. 6(b) also corroborates the formation of $^{79}Kr@C_{70}-C_{70}$. Similar results for $C_{60}$ ($C_{70}$) fullerenes were obtained also in the elution behavior of the $^{127}$Xe radioactivity for the samples of $C_{60}$ ($C_{70}$) mixed with KI.[31] Activities of $^{79}$Kr on the eluent fractions were collected and integrated for the decay of $^{79}$Kr. Total activities of $^{79}$Kr incorporated within fullerenes were estimated to be of the magnitude of 200–300 Bq/mg. On the other hand, the amount of $^{127}$Xe incorporated within fullerenes was estimated to be of the magnitude of 20–30 Bq/mg. The amount of endohedral fullerenes of $^{79}$Kr and $^{127}$Xe, which were produced here, is then estimated to be about $10^{10}$ molecules. Quite recently, Gadd *et al.* presented evidence for the formation of endohedral fullerenes of Xe atoms by using the prompt-gamma recoil method with neutron activation.[34] The result seems to be similar, but no evidence of the formation of their polymers has been presented.

### B. Molecular dynamics simulation

In order to rationalize the experimental results, *ab initio* molecular dynamics (MD) simulations for the collision between several atoms and the $C_{60}$ cage were carried out, and the possibility of encapsulation was investigated. We use an *ab initio* MD method based on the all-electron mixed-basis approach which uses both atomic orbitals (AO) and plane waves (PW) as the basis set within the framework of the local density approximation (LDA). So far, we have carried out similar simulations of Li- and Be-insertions into $C_{60}$ (Refs. 32 and 30) by using analytic Slater-type atomic orbitals. Our recent calculations involving K, Cu, As, Kr, Xe insertions have used atomic orbitals determined numerically by a standard atomic code.[31,35] For example, we adopt 313 (or 323) numerical atomic orbitals for the K, Cu, As, Kr (Xe) system as well as 4169 plane waves corresponding to a 7 Ry cutoff energy. For dynamics, we assume an adiabatic approximation where the electronic structure is always in the ground state. We use a supercell composed of $64\times64\times64$ meshes, in which 1 a.u.$=0.529\,18$ Å corresponds to 2.7 meshes. For every simulation concerning atomic insertion, we put one $C_{60}$ molecule, which is stationary at $t=0$, and one atom moving with a given initial velocity toward the center of the uppermost six-membered ring (hereafter we shall call this six-membered ring, $u$-$C_6$) of $C_{60}$ vertically. The initial position of an inserting atom is set at 1.5 Å above the center of $u$-$C_6$. The basis time step is typically set to $\Delta t=4$ a.u.$\sim$0.1 fs, and perform five to six steepest descent (SD) iterations after each updation of atomic positions in order to converge the electronic states. The atomic dynamics is based on the Newtonian equations.

First, in the case of a K collision at 100 eV with $C_{60}$, the K atom passes through the $u$-$C_6$. However, $C_{60}$ in this case does not recover its initial configuration even after 125 fs from the collision and the cage is still open around the collision site as seen in Fig. 7. This is because the chemical reaction between K and the carbon atoms is very strong compared to the case between noble-gas and carbon atoms. Although the K atom will be encapsulated eventually, the process takes a much longer time. In fact, we observed a small amount of the coalesced products, such as $V@C_{60}$ or $Mn@C_{60}$. Similar results were obtained in the calculations for the collision between V, Cu atoms and the $C_{60}$ cage. Therefore, we conclude that the creation rate of $M@C_{60}$ (M=alkali, alkali-earth, and transitional metals) can be much lower than that of $Kr@C_{60}$ ($Xe@C_{60}$). This is certainly consistent with the present experimental results.

Second, we performed the following three types of simulations in the case of As: (A) insertion of the As atom through a six-membered ring of $C_{60}$; (B) insertion between one As atom and one C atom of $C_{60}$; and (C) structural stability of $AsC_{59}$. In (A), the As atom with various kinetic energies vertically hits the center of a six-membered ring of $C_{60}$. We found that an As atom can penetrate into $C_{60}$ easily with a relatively low kinetic energy, just like noble-gas atoms,[31] when its initial energy is greater than 70 eV. This can be due mainly to the covalent interaction between carbon and arsenic atoms, which is weaker and more short-range than ionic interactions. In (B), we shift one of the C atoms of

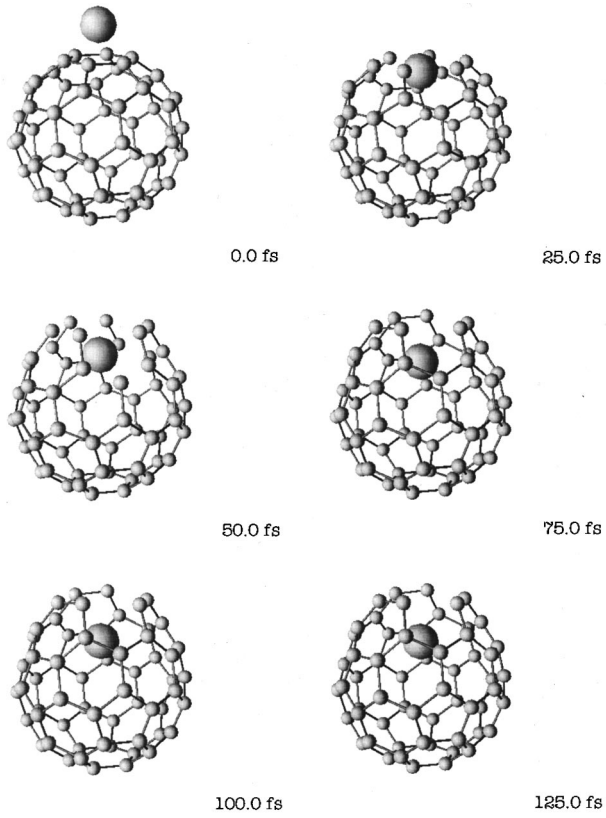


FIG. 7. Simulation of K hitting the center of a six-membered ring of $C_{60}$ with a kinetic energy of 100 eV. Here, the local skeleton disappears from the figure when the bond length is elongated by more than 1.5 Å.

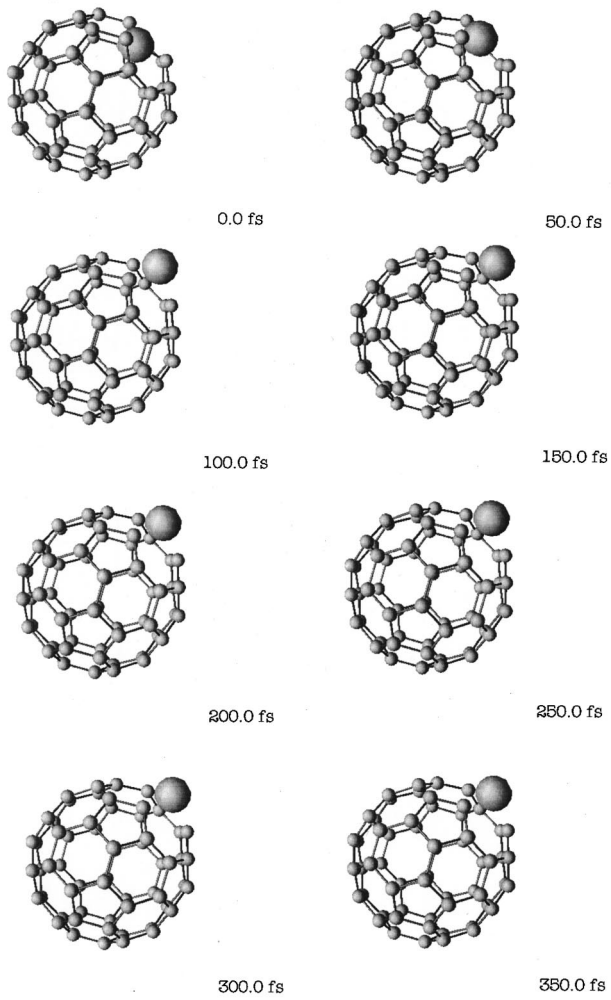


FIG. 8. Simulation of the structural stability of $AsC_{59}$: Change from an unstable inner side (0.53 Å inward from the cage sphere) with an initial KE of 0 eV to a final stabilized configuration in $AsC_{59}$.

$C_{60}$ outward by 1.3 Å (at radius 4.9 Å) and put additionally one As atom on the same radial axis by 1.3 Å inward from the original C position (at radius 2.2 Å). Then, starting the simulation with zero initial velocity, we found that there is a strong force acting on the As atom to accelerate it outward and, as a result, to repel the outward C atom still further outward. This force is, however, not due to the interaction with the outer C atom, but it exists even in the absence of the outer C atom. In fact, if we perform a similar simulation without the outer C atom, the inner As atom (initially put at 0.53 Å inward from the cage sphere) starts going outward as if it would leave the cage. This is actually the simulation (C) we carried out after 100 fs at 0.73 Å from the cage sphere. However, the As atom comes back again and stops finally, as seen in Fig. 8. Note that, in our simulation, there is a little energy loss caused by the SD algorithm for electronic states. The final position of the As atom is at 0.50 Å from the cage sphere (at radius 4.06 Å). Thus we conclude that the As atom, when put inside the cage, is quite unstable, and it has a strong tendency to repel the closest C atom of $C_{60}$, being stabilized slightly outside the cage sphere after the removal of the closest C atom.

Third, in the case of noble-gas atoms, Kr with an initial kinetic energy (KE) greater than 80 eV and Xe with an initial KE greater than 130 eV penetrate into the cage of $C_{60}$ through the center of $u$-$C_{60}$ without difficulty, although a KE higher than 150 eV for Kr and 200 eV for Xe allow the noble-gas atom to go out again from the opposite side of the cage.[31] Figure 9 shows several snapshots of the Kr insertion with 130 eV KE. In the figure, after the Kr atom has first touched $u$-$C_6$, carbon atoms are pushed to open $u$-$C_6$ and the Kr atom goes through (of course, according to the momentum-conservation law, most of the kinetic energy of the colliding particle transfers very quickly to the $C_{60}$ as a whole in a way each carbon atom tends to move in the same direction with a same speed). But $u$-$C_6$ soon recovers its initial configuration. Finally, the Kr atom collides with the other side of $C_{60}$ and it is bounced towards the center of the cage. With a relatively low initial KE (typically $\leqslant$300 eV for Xe and Kr), $C_{60}$ shows a tendency to recover its original shape within the simulation period. The result of a simulation changes, of course, according to the impact energy, impact point and angle. In case of higher initial kinetic energies ($\geqslant$300 eV for Xe and Kr), six $C_2$ losses occur simultaneously from the upper side of $C_{60}$. If a noble-gas atom is inserted toward off-center positions of a six- or five-membered ring, the damage suffered on $C_{60}$ increases significantly.

All these results of our simulations are summarized in Table II.

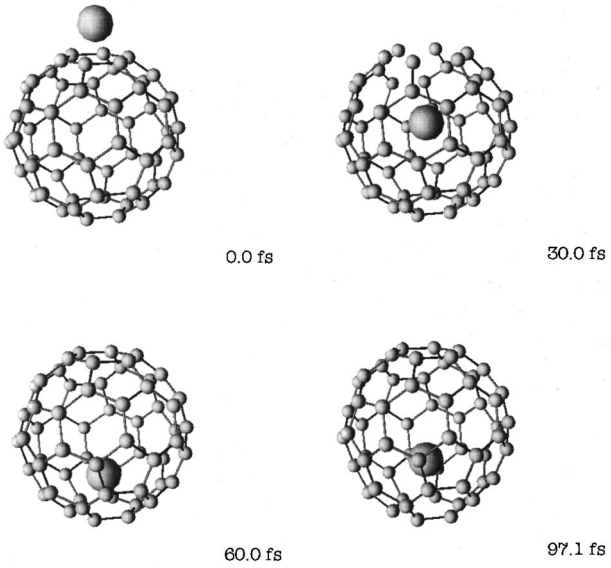


FIG. 9. Simulation of Kr hitting the center of a six-membered ring of $C_{60}$ with a kinetic energy of 120 eV. The local skeleton disappears from the figure when the bond length is elongated by more than 1.5 Å.

### C. Scenario of foreign atom implantation

All the experimental results that have been presented here support the following scenario: Several radioactive nuclides are produced by $(d,n)$ $(d,2n)$, or $(\gamma,n)$ reactions. The kinetic energies (KE) of the radionuclides are almost of the same order of magnitude even in the different nuclear reactions. As the form of the emitted neutron spectrum is expected to be approximately Maxwellian and the average neutron KE seems to be about 2–3 MeV, while the initial KE of the recoiled nuclides is estimated to be about a few hundred keV (even if the reaction is accompanied by two neutron emissions). The energetic nuclides should destroy the fullerene cages because the KE is estimated to be of a quite different order of magnitude than the energies (eVs) of molecular bonding. Therefore, the atoms being produced escape from their own material due to the KE of about a few hundred kiloelectron volts. Then, the kinetic energies are reduced in the sample to a magnitude which is appropriate for the fusion. Finally, the radionuclides hit the $C_{60}$ cages and stop in the cage (formation of endohedral fullerene or heterofullerene) and, furthermore, the shock produces fullerene polymers by interaction with a neighboring fullerene cage.

TABLE II. Summary of the results of simulated atomic collisions at the center of a six-membered ring ($u$-$C_6$). The initial kinetic energy (KE) is given in units of eV for each case. Blanks indicate that no calculation has been performed.

| | Li,Be | K | V | Cu | As | Kr | Xe |
|---|---|---|---|---|---|---|---|
| Trapped outside | 1 | | | 50 | | | |
| Reflected | | 50 | | | | | |
| $u$-$C_6$ opened | | 100 | 100–150 | 100 | 50 | | |
| Encapsulation | 5 | | | 150 | 80 | 80–150 | 130–200 |
| Passed through | | 160 | | | 160 | 150– | 200– |
| $C_2$ losses | | | | | | 300– | 300– |

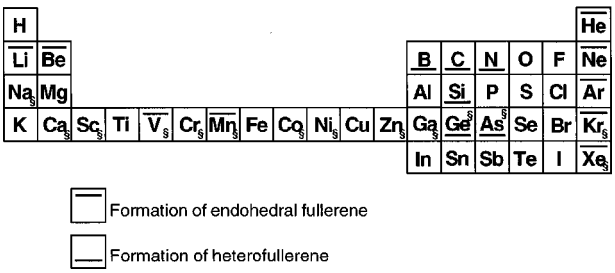


FIG. 10. Schematic view of a partial periodic table. In this figure, (§) indicates the elements investigated in the present work. The formation of endohedral fullerenes of $C_{60}$ or $C_{70}$, which has been confirmed by using several techniques, is indicated by overbars, and that of heterofullerenes of $C_{60}$, which were doped in the cage, is indicated by underbars.

### D. Systematic trend of atom-doped fullerenes

In the present study, several fourth-cycle elements in a periodic table have been investigated by a recoil implantation following nuclear reactions. However, some elements, such as K, Fe, Cu, Se, and Br atoms, could not be investigated mostly due to a lack of an appropriate half-life of radionuclide and of an abundance of their characteristic $\gamma$-ray. A schematic view of a portion of the periodic table is shown in Fig. 10. In the figure, elements which are experimentally confirmed to combine with fullerene cages are shown by underbars (substitutionally doping heterofullerenes) and overbars (endohedrally doping fullerenes). It is interesting to note that only elements in groups 4B and 5B form substitutionally doping heterofullerenes.

There is a slight shift in the eluent peaks of the UV chromatogram and in the radioactive populations. That is, the peaks in the objective radioactivities are shifted to later times from the peaks in the UV chromatogram (fullerene populations). The same trend was observed in the elution behavior of the metallofullerene extraction, such as $^{7}Be@C_{60}$[30] and $^{159}Gd@C_{82}$.[36] Why does the delay occur in the retention time between the absorbance of the UV chromatogram and the $\gamma$-counting rate of the radioactivities? In these cases, it seems that the electron density of the endohedral fullerene or of the heterofullerene is distorted by the atom trapped in the cage. The distorted electrons may change the magnitude of the interaction between the endohedral fullerene or heterofullerene and the resin inside the column.

## V. CONCLUSION

In this study, the formation of atom-doped fullerenes has been investigated by using several types of radioactivity which are produced by nuclear reactions. It was found that noble-gas elements, like Kr and Xe, as well as 4B and 5B group elements, like Ge and As, remained in the $C_{60}$ portion after a HPLC process. Though a small number of $^{48}V$ and $^{52}Mn$ atoms remained in the $C_{60}$ population, most of the other elements, such as alkali, alkali-earth, and transitional metals, could not be detected in the $C_{60}$ portion. These facts suggest that the formation of endohedral fullerenes ($Kr@C_{60}$, $Xe@C_{60}$ and of their polymers) and heterofullerenes ($AsC_{59}$, $GeC_{59}$ and of their polymers) can be possible by a recoil process following nuclear reactions, while

other elements (Na, Ca, Sc, etc.) may destroy most of fullerene cages due to strong chemical reactivity between atoms and fullerenes. By carrying out *ab initio* molecular-dynamics (MD) simulations on the basis of the all-electron mixed-basis approach, we confirmed that the insertion of Kr (and Xe) atoms into $C_{60}$ through six-membered rings and, furthermore that the formation of substitutionally doped heterofullerenes with an As atom is possible. These experimental and theoretical results indicate that chemical reactivity or inactivity seems to play an important role in the formation of foreign-atom-doped fullerenes.

## ACKNOWLEDGMENTS

The authors are grateful to the technical staff of the Laboratory of the Nuclear Science and the Cyclotron Radio-Isotope Center for beam-handling and to the technical staff working at IMR, Tohoku University for their continuous support for the supercomputing facilities. This work was supported by the Grant-in-Aid for Co-operative Research No. 10640535 and No. 10874041 from the Ministry of Education, Science and Culture of Japan.

[1] H. Kroto *et al.*, Nature (London) **318**, 162 (1985).
[2] W. Krätschmer *et al.*, Nature (London) **347**, 354 (1990).
[3] Y. Chai *et al.*, J. Phys. Chem. **95**, 7564 (1991).
[4] R. D. Johnson *et al.*, Nature (London) **355**, 239 (1992).
[5] J. H. Weaver *et al.*, Chem. Phys. Lett. **190**, 460 (1992).
[6] H. Shinohara *et al.*, J. Phys. Chem. **96**, 3571 (1992).
[7] H. Shinohara *et al.*, Nature (London) **357**, 52 (1995).
[8] M. Takata *et al.*, Nature (London) **377**, 46 (1995).
[9] W. Sato *et al.*, Phys. Rev. Lett. **80**, 133 (1998).
[10] K. Sueki, K. Akiyama, K. Kikuchi, and H. Nakahara, Chem. Phys. Lett. **291**, 37 (1998).
[11] L. M. Roth *et al.*, J. Am. Chem. Soc. **113**, 6298 (1991).
[12] Y. Huang and B. S. Freiser, J. Am. Chem. Soc. **113**, 9418 (1991).
[13] S. W. McElvany, J. Phys. Chem. **96**, 4935 (1992).
[14] T. Guo, C. Jin, and R. E. Smalley, J. Phys. Chem. **95**, 4948 (1991).
[15] H. J. Muhr, R. Nesper, B. Schnyder, and R. Kötz, Chem. Phys. Lett. **249**, 399 (1996).
[16] T. Pradeep, V. Vijayakrishnan, A. K. Santra, and C. N. R. Rao, J. Phys. Chem. **95**, 10564 (1991).
[17] J. F. Christian, Z. Wan, and S. Anderson, J. Phys. Chem. **96**, 10597 (1992).
[18] M. Pellarin *et al.*, Chem. Phys. Lett. **277**, 96 (1997).
[19] C. Ray *et al.*, Phys. Rev. Lett. **80**, 5365 (1998).
[20] W. Branz *et al.*, J. Chem. Phys. **109**, 3425 (1998).
[21] M. Saunders *et al.*, Science **271**, 1693 (1996).
[22] T. Braun and H. Rausch, Chem. Phys. Lett. **237**, 443 (1995).
[23] T. Braun and H. Rausch, Chem. Phys. Lett. **288**, 179 (1998).
[24] G. E. Gadd *et al.*, Chem. Phys. Lett. **270**, 108 (1997).
[25] T. Ohtsuki *et al.*, J. Am. Chem. Soc. **117**, 12869 (1995).
[26] T. Ohtsuki, K. Masumoto, K. Kikuchi, and K. Sueki, Mat. Sci. Eng. **217/218**, 38 (1996).
[27] K. Masumoto *et al.*, J. Rad. Nucl. Chem. **239**, 201 (1999).
[28] T. Ohtsuki *et al.*, J. Rad. Nucl. Chem. **239**, 365 (1999).
[29] T. Ohtsuki, K. Masumoto, T. Tanaka, and K. Komatsu, Chem. Phys. Lett. **300**, 661 (1999).
[30] T. Ohtsuki *et al.*, Phys. Rev. Lett. **77**, 3522 (1996).
[31] T. Ohtsuki *et al.*, Phys. Rev. Lett. **81**, 967 (1998).
[32] K. Ohno *et al.*, Phys. Rev. Lett. **76**, 3590 (1996).
[33] *Table of Isotopes*, edited by R. B. Firestone *et al.* (Wiley, New York, 1996), Vol. I.
[34] G. E. Gadd *et al.*, J. Am. Chem. Soc. **120**, 10322 (1998).
[35] K. Shiga, Modell. Simul. Mater. Sci. Eng. **7**, 621 (1999).
[36] K. Kikuchi *et al.*, J. Am. Chem. Soc. **116**, 9775 (1994).